Journal of Computational Physics **158,** 225–238 (2000)
doi:10.1006/jcph.1999.6416, available online at http://www.idealibrary.com on IDEAL®

Convergence Tests for the Piecewise Parabolic Method and Navier–Stokes Solutions for Homogeneous Compressible Turbulence

Igor V. Sytine,* David H. Porter,* Paul R. Woodward,* Stephen W. Hodson,† and Karl-Heinz Winkler†

**Laboratory for Computational Science and Engineering, University of Minnesota, Minneapolis, Minnesota 55455; † Los Alamos National Laboratory, Los Alamos, New Mexico 87545*
E-mail: {sytine, dhp, paul}@lsce.umn.edu, {swh, khw}@lanl.gov

Received December 7, 1998; revised November 16, 1999

The need to simulate fully developed turbulence with wide range of scales led us to use the Piecewise Parabolic Method (PPM) to solve the Euler equations of motions. To obtain data for 3-D homogeneous compressible decaying turbulence numerical simulations were performed on computational meshes of up to 1024^3 zones. These data were compared with data obtained by solving the Navier–Stokes (NS) equations. Results of studying the kinetic energy, enstrophy, and the energy power spectra with different resolutions are presented for both the PPM and NS data. The results of the comparison show convergence of the PPM and NS solutions to the same limit.

Key Words: turbulence modeling; homogeneous compressible turbulence; Piecewise Parabolic Method; subgrid-scale models.

1. INTRODUCTION

Over the last few years the Laboratory for Computational Science and Engineering (LCSE) has been simulating the development and decay of compressible turbulence in three-dimensional (3-D) periodic flows [1–4] using the Piecewise Parabolic Method (PPM) [5–7] to solve the Euler equations of fluid dynamics. These simulations rely on the numerical dissipation of this difference scheme to transform turbulent kinetic energy into heat on the finest scales, while leaving the larger scales unaffected. The effectiveness of this approach has been investigated earlier [3, 4] as well as the features of the numerical dissipation [8, 9].

It has long been believed that Navier–Stokes computations are the preferred way to simulate turbulence. While it is true and ideal, unfortunately the complexity of the computations is so far beyond the current capabilities of the modern computers, that it has forced us to depart from this approach and to use Euler schemes instead.

0021-9991/00 $35.00

To show the validity and effectiveness of using Euler schemes and PPM as one of them for turbulence modeling, convergence tests and comparison with the Navier–Stokes (NS) solutions were performed in 2-D.

Convergence tests of 2-D PPM of compressible turbulence [2–4] showed that the velocity power spectra of PPM agree within 10% in models resolved on meshes ranging from 128^2 to 1024^2. Comparisons of resolved NS computations on the same problem on a given grid showed that computed data in both NS and PPM runs agreed at large scales. Structures in the runs are identical with respect to their location and shape although they are visually slightly blurred by viscosity in the 2-D NS run. As the meshes are refined, these simulations all converge to the same high Reynolds number limit, but the Euler simulations reach this limit much faster.

In spite of long use and successful applications of the PPM [15–17, 21, 22] there is still a need to continue comparative analysis of PPM and NS data in 3-D and with higher resolution.

Increases in computer speed, storage, and our ability to analyze significant volumes of data allowed us to proceed with comparisons of PPM and NS computations for the 3-D case with mesh size up to 512^3 and even up to 1024^3 for PPM. Such comparisons and convergence tests will be the focus of this paper.

2. NUMERICAL SIMULATIONS

The data for the PPM run of 1024^3 which are analyzed in this paper are the result of the collaboration of research teams at LCSE and Los Alamos National Laboratory (LANL), where the simulations were carried out by using Silicon Graphics Origin-2000 computing hardware. The PPM code and shared-memory multi-processor cluster computer architecture allowed us to achieve a parallel efficiency of over 90% on 128 Origin-2000 processors, with a total sustained performance of 14 Gflops/s .

The NS run of 512^3 was performed at the National Center for Supercomputing Applications (NCSA) on 64 processors of the Silicon Graphics Origin-2000 machine.

Our simulations focused on the simplest case of homogeneous isotropic turbulence for which periodic boundary conditions are appropriate. We began with a uniform gas at rest in a periodic cubical box, with the length of each side equal to 2π. Density was unity and the ratio of specific heat was $\gamma = 1.4$ (as appropriate for air).

Velocity perturbations were introduced by randomly oriented, isentropic, sinusoidal sound and shear waves concentrated on the large scales with an rms Mach number of one-half. The initial condition has a velocity power spectrum $k^4 \exp(-k/k_0)^2$, with $k_0 = 2$, which places 99% of the energy in modes with k less than 4. These initial disturbances have wavelengths chosen from a distribution centered on half the width of the simulation cube. Their amplitudes were chosen to produce a root mean square velocity magnitude corresponding to a Mach number of one-half. The fraction of the compressible component of the velocity to its solenoidal component was $1/10$.

The energy-containing scale of this initial state was π, or half the size of the periodic box. The wave crossing time of the energy containing scale in the initial state would be our unit of time. Such choice of units allows us to be consistent with our previous work as well as with the standard conventions used by others in modeling incompressible flows of this type.

The decaying case has been modeled, so the flow is not driven and the typical magnitude of velocity decays in time. We provide the data for runs up to time $t = 2$, which contains the time interval with maximum enstrophy.

2.1. PPM Euler simulations. The PPM was originally developed to simulate the unsteady flows with strong shock often found in astrophysics, such as supernova explosions and supersonic jets. It used the ideas of Bram van Leer [18] to extend the method of Godunov [19] to a higher formal order of accuracy. Its success comes from the combination of several techniques. Given zone-averaged data, a high-order interpolation is used to construct descriptions of the relevant variables everywhere in space, providing accuracy in regions of smooth flow. Monotonicity constraints are applied to ensure that the advection of monotone data produces monotone results.

The importance of monotonicity [23] has been the theme of the work on computing turbulent flows that has been done by J. P. Boris, F. F. Grinstein, and co-workers over the last ten years [24, 26]. They have done numerous tests of the concept they call MI-LES. Furthermore, the recent work by C. Fureby and F. F. Grinstein has shown that monotone algorithms have the right properties for subgrid models [25]. Decaying homogeneous turbulence computed with various monotone methods, a Navier–Stokes code, an Euler code, and then also with MI-LES, showing the proper spectrum, are discussed in Refs. [27, 28].

Several additional features of PPM contribute to its effectiveness. Discontinuity detection algorithms are used to modify the interpolation in zones near discontinuities in order to better represent these structures. This helps to prevent numerical viscosity from smearing discontinuities as they move through the computational grid. Shock detection is also performed so that an appropriate amount of localized numerical dissipation is added only to those zones in shocks.

Multi-dimensional flows are solved by applying a one-dimensional scheme in alteration according to the directional-splitting algorithm of Strang [20]. In our case this provides the second-order accuracy.

The amplitude of the effective kinematic viscosity of PPM on a given scale on a given computational mesh was analyzed by Porter and Woodward [9]. It was found that the effective Reynolds number for flows on a given length scale varies as N^3, where N is the number of computational cells across the wavelength of the structure in question.

For the case of the 1024^3 computation, the integral scale at time $t = 2$ was spanned by 262 computational cells which led to an effective Reynolds number $Re = 3.6 \times 10^7$. This large value of Re represents the extremely small amplitude of the numerical dissipation of PPM relative to the inertial terms on the largest scales of these well-resolved simulations. The effective Prandtl number for our simulation is near unity [9].

We adopt the fluid dynamical equations for a perfect polytropic inviscid gas, which can be written as

$$\frac{\partial \rho}{\partial t} + \nabla \cdot (\rho \mathbf{u}) = \mathbf{0} \tag{1}$$

$$\frac{\partial \mathbf{u}}{\partial t} + \mathbf{u} \cdot \nabla \mathbf{u} = -\frac{\mathbf{1}}{\rho} \nabla \mathbf{P} \tag{2}$$

$$\frac{\partial (\rho E)}{\partial t} + \nabla \cdot (\mathbf{u} \rho \mathbf{E}) = -\nabla \cdot (\mathbf{u} \mathbf{P}), \tag{3}$$

where ρ is the density, and $\mathbf{u}$ is the velocity, and where the total energy density per unit mass $E = \frac{1}{2}\mathbf{u^2} + \mathbf{P}/(\gamma - \mathbf{1})\rho$. Here $\mathbf{P}$ is the pressure, and $\gamma = 1.4$ is the adiabatic index with $\mathbf{P} = (\gamma - 1)\rho\epsilon$. The internal energy is related to the temperature T and heat capacity at constant volume c_v by $\epsilon = c_v T$. Finally, the speed of sound c is given by $c^2 = \gamma(\gamma - 1)\epsilon$.

The velocity field is decomposed into its solenoidal $\mathbf{u_s}$ and compressional $\mathbf{u_c}$ components as $\mathbf{u} = \mathbf{u_s} + \mathbf{u_c}$ with $\nabla \cdot \mathbf{u_s} = \mathbf{0}$ and $\nabla \times \mathbf{u_c} = \mathbf{0}$.

The initial rms Mach number is one-half. We chose units so that the mean density ρ and initial mean speed of sound c_0 were both equal to unity.

The purpose of an Euler solver like PPM is to approximate on a given grid the limit solution of the Navier–Stokes equations as the viscosity and thermal conductivity tend to zero. To establish how well PPM is doing this job in the context of these 3-D turbulent flows we generated for comparison a sequence of resolved Navier–Stokes solutions with Prandtl number unity and with increasingly large Reynolds numbers.

2.2. Navier–Stokes simulations. The series of NS runs was simulated with computational meshes of increasing resolution and the results were compared with PPM runs on these same grids. The levels of viscosity and thermal conductivity were clearly and unequivocally specified for NS runs, while for PPM the numerical viscosity and thermal conductivity decreased automatically as the mesh resolution increased. The Prandtl number was equal to one in all of these runs. A PPM directionally split Rieman solver was used with the addition of the Navier–Stokes viscous term in the right hand side of Eq. (2) in the form $\partial_k\{\eta(\partial_k v_i + \partial_i v_k - 2/3\delta_{ik}\partial_l v_l)\} + \partial_i(\zeta\,\partial_l v_l)$. Assuming the bulk viscosity is $\zeta = 0$, we are changing the dynamic viscosity η.

An additional energy flux due to thermal diffusivity χ is present as a source term in the energy Eq. (3) $\sim \chi \nabla T$. We are keeping the thermal diffusivity as a constant.

For NS simulations at each mesh resolution we attempted to impose the minimum level of Navier–Stokes dissipation that was consistent with an accurate numerical solution. We varied the dynamical viscosity coefficient in the Navier–Stokes solver while keeping the ratio of the integral and dissipative scales the same. In order to do so we kept the variation of the dynamic viscosity coefficient proportional to $N^{-4/3}$, where N is the size of the mesh [14]. Note that in this case the ratio of the dissipative scale $\lambda_d = (\nu/ul)^{3/4} l$ and the size of the mesh zone Δx remain constant.

The viscosity coefficient consistent with an accurate numerical solution was set for a grid of 64^3 cells by demanding that the velocity power spectrum of this solution not change upon grid refinement.

To execute the series of NS runs it was necessary to choose the initial viscosity, which would decrease with each mesh size doubling according to the scaling described above. For the series of low resolution single precision runs of sizes 32^3, 64^3, and 128^3 for dynamical viscosity coefficients varying from 0.001 to 0.0001 it was concluded that the dynamical viscosity coefficient $\nu = 0.0005$ is an appropriate value. At this viscosity the velocity power spectra for meshes 64^3 and 128^3 coincide nearly up to the Nyquist frequency of the lower resolution run. At the same time for the 32^3 grid the Navier–Stokes solution is clearly under-resolved. The increase of the viscosity to 0.001 allowed us to obtain resolved NS solutions for all three mesh sizes (see Fig. 1). Some insignificant flattening of the spectra near the Nyquist frequency was due to single precision of our initial runs. In following double precision runs it was not observed.

The combination of resolved and under-resolved runs, which were done in double precision, we can see in Fig. 2. For viscosity coefficient 0.0005 we fully resolve flow at mesh size of 64^3; at the same time we observe flattening of the spectra near the Nyquist frequency for mesh 128^3. This flattening disappears when we decrease the viscosity. We should note that curves of the kinetic energy dissipation with time for all meshes coincide with a high

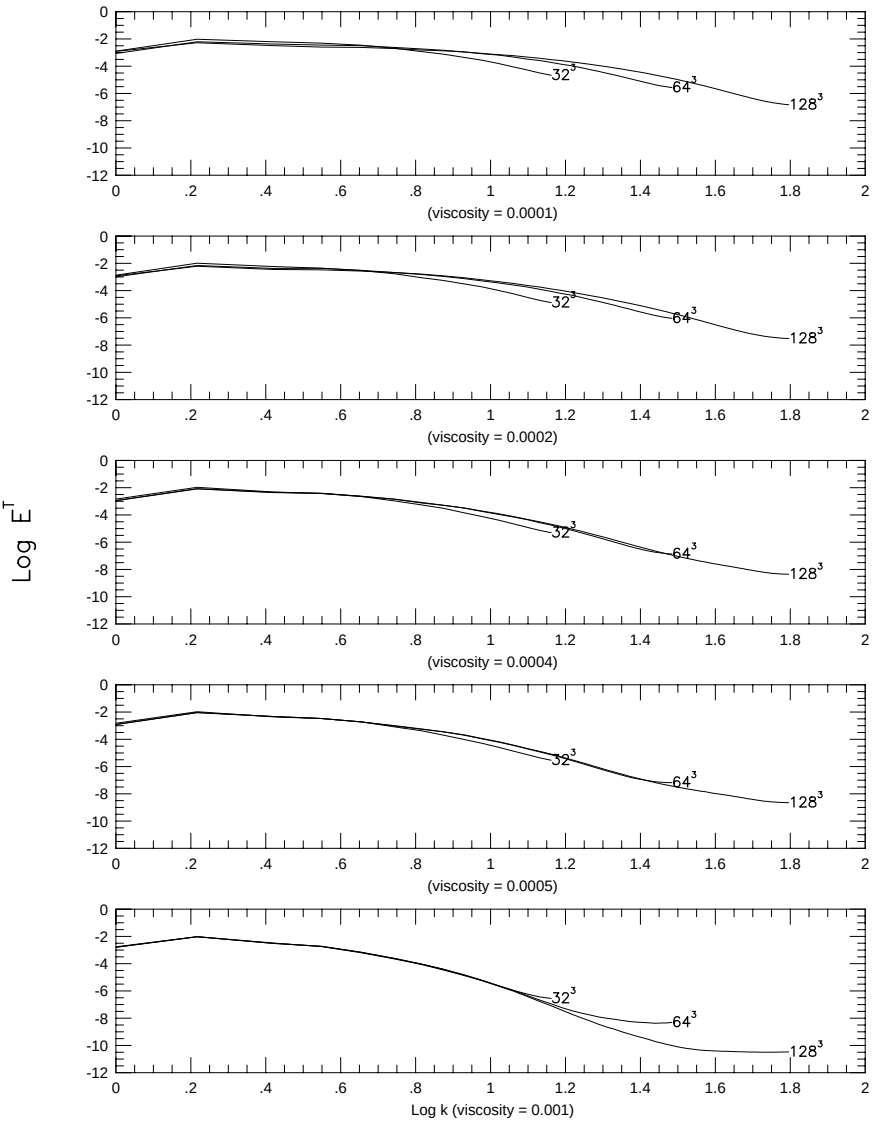

FIG. 1. Velocity power spectra at $t = 2$ for a series of runs with different choices of the dynamic viscosity coefficient in the Navier–Stokes solver. Mesh sizes of 32, 64, 128 zones on a side were used for each choice of viscous coefficient.

accuracy, proving that we indeed have resolved Navier–Stokes calculations. Moreover, we can see in Fig. 3 that increase of the resolution from 64 to 128 for viscosity $\eta = 0.0005$ provides an indistinguishable difference in the decay of the kinetic energy. For the same viscosity any following growth of the resolution leads to an increase of the error in the Nyquist frequency neighborhood.

3. RESULTS AND DISCUSSION

We begin by presenting the results obtained for enstrophy, which is defined as $\Omega_1^s = \int_0^\infty k^2 E^s(k)\, dk$, Fig. 4, where $E^s(k)$ corresponds to the kinetic energy for the solenoidal

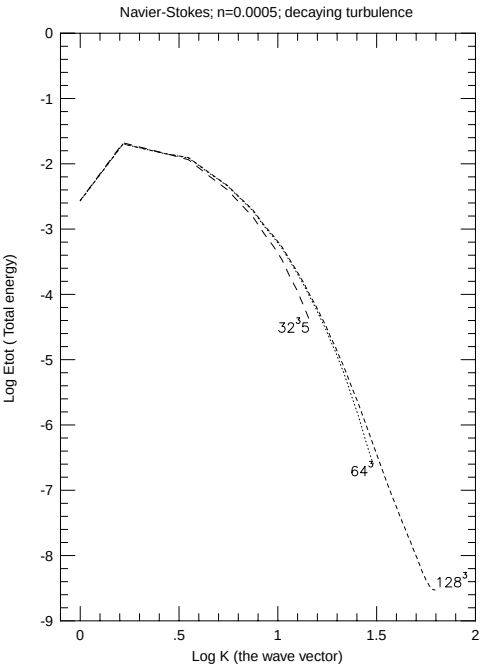

FIG. 2. Velocity power spectra at $t = 2$ for a series of runs with the dynamic viscosity coefficient $\eta = 0.0005$. Mesh sizes of 32, 64, 128 zones on a side.

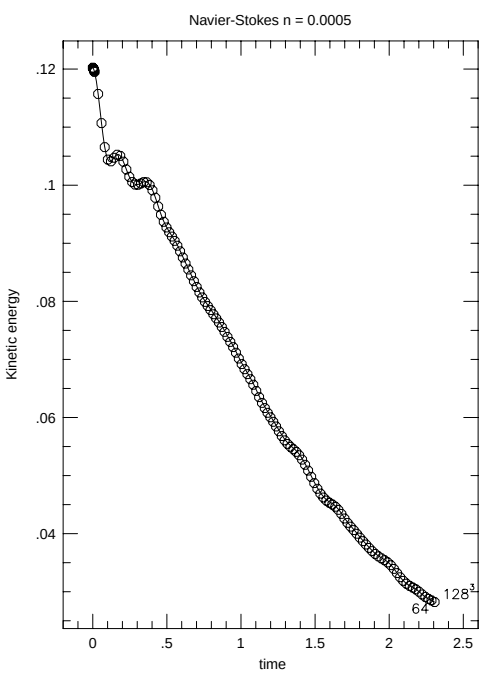

FIG. 3. Decay of the kinetic energy in time for mesh sizes 64 and 128 and constant viscosity coefficient $\eta = 0.0005$.

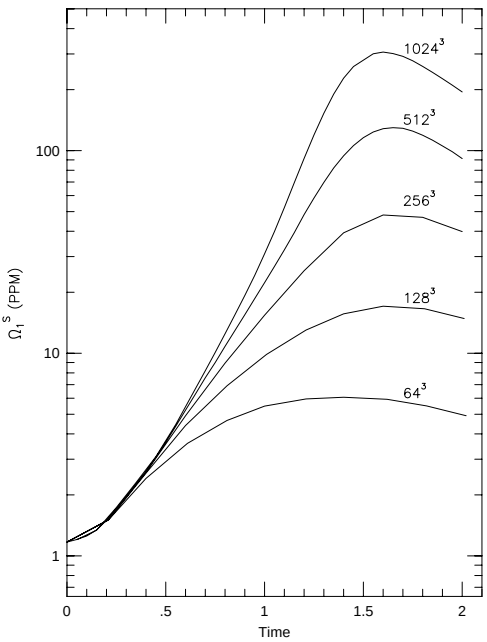

FIG. 4. The enstrophy time dependence for decaying compressible turbulence. The initial Mach number is 0.5. Results for the PPM Euler code on meshes of 64^3, 128^3, 256^3, 512^3, and 1024^3 cells are shown. In all cases, the enstrophy peaks at around time 1.5.

component of velocity in Fourier space integrated on a sphere of radius k. Similar mesh size dependency for both PPM and NS calculations is observed. The maximum of the enstrophy is reached earlier for mesh sizes 64^3 and 128^3, while the maximum for 256^3 was reached later. With further increases in mesh size to 512^3 and 1024^3 the enstrophy maximum appears at slightly earlier times.

The enstrophy for our series of NS runs, Fig. 5, is lower in value and seems strongly damped by high viscosity in low resolution runs. In both PPM and NS calculations the enstrophy behavior is consistent with the expectation that the enstrophy tends to infinity at a finite time in a zero viscosity limit [14]. A significant growth of enstrophy is observed when the viscosity is decreased, while the time of maximum enstrophy remains roughly the same.

For both our PPM and NS simulations the system is past its maximum of the enstrophy by time two in our time units. Therefore we have chosen to compare our results from these simulations at time 2. In all runs all available modes have been excited by this time, energy has reached the dissipation scale, and the flows are fully turbulent.

In order to measure the intensity of compressive motions, we examine the quantity $\Omega_1^c = \int_0^\infty k^2 E^c(k)\, dk$, the second moment of the power spectrum for compression energy, where $E^c(k)$ corresponds to the kinetic energy for the compressive component of velocity in Fourier space integrated on a sphere of radius k. Figure 6 represents a comparison for this quantity of PPM and NS runs. The step on the curves corresponds to shock formation in compressible flow. We can see that both methods show similar qualitative results for this parameter. The time when all shocks in a volume have already formed is about $t = 0.4$ and it is the same for both the PPM and NS runs in Figs. 6 and 7.

The dynamics of kinetic energy with time for PPM is represented in Fig. 8. The comparison of the kinetic energy time dependence for the PPM and NS runs is presented in

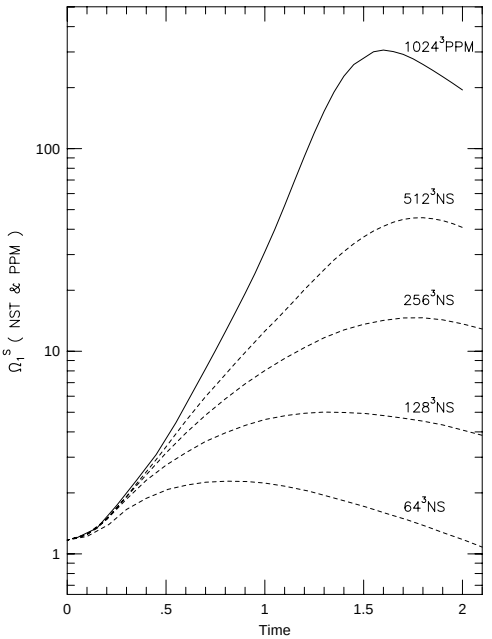

FIG. 5. The enstrophy time dependence for decaying compressible turbulence, with initial Mach number = 0.5. Results for well-resolved Navier–Stokes simulations on grids of 64^3, 128^3, 256^3, 512^3 are shown, corresponding to Reynolds numbers of 500, 1260, 3175, and 8000, respectively. Results for the PPM Euler code on a 1024^3 grid are also shown for comparison.

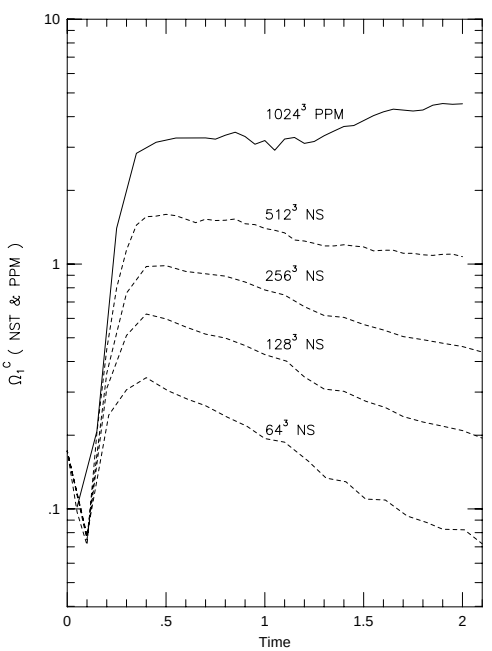

FIG. 6. The time evolution of the quantity Ω_1^c (the second moment of the power spectrum for compression energy), which measures the intensity of compressive motions. Navier–Stokes and the 1024^3 PPM Euler runs are compared. The initial Mach number = 0.5. Mesh sizes for NS runs vary from 64 up to 512 zones on a side. The PPM run uses a 1024^3 grid.

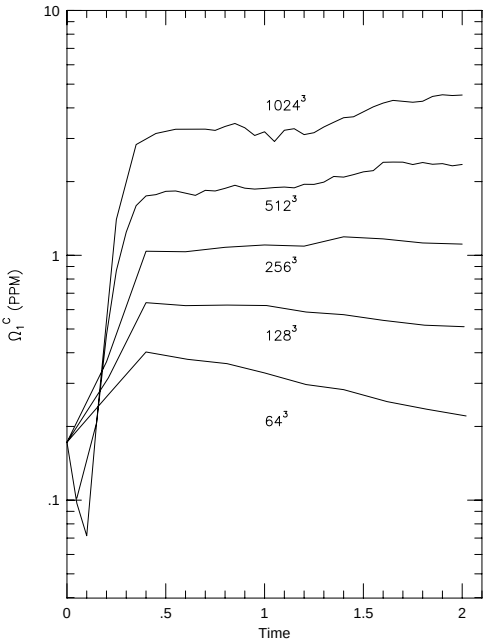

FIG. 7. The time evolution of the quantity Ω_1^c (the second moment of the power spectrum for compression energy), which measures the intensity of compressive motions in five PPM Euler simulations of decaying compressible turbulence. The initial Mach number is 0.5, and grids of 64^3, 128^3, 256^3, 512^3, and 1024^3 are used.

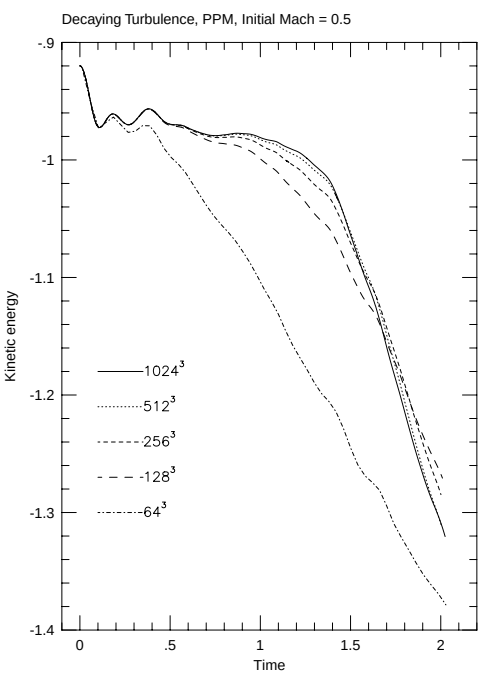

FIG. 8. The kinetic energy time dependence for decaying compressible turbulence. The initial Mach number is 0.5. Mesh size changes from 64 up to 1024 zones per side of the cube. Computing method is PPM.

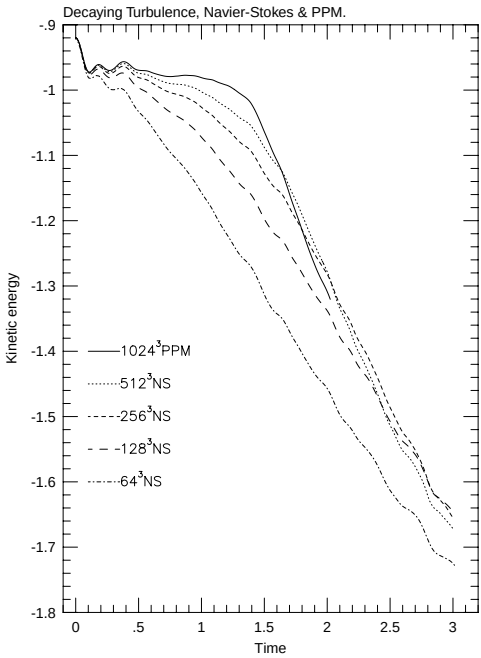

FIG. 9. The kinetic energy time dependence for decaying compressible turbulence. The initial Mach number is 0.5. Mesh size changes from 64 up to 512 zones per side of the cube for Navier–Stokes solver. The 1024^3-zone PPM solution is presented for comparison.

Fig. 9. One can clearly see the convergence of the kinetic energy time history for the NS runs towards that for PPM. We can see that the rate of decay of the kinetic energy at the later times becomes steeper as the mesh size increases, while still converging towards the value for PPM, which is the steepest at these later times. In both cases there is a bend in the time history curve near time about $t = 1.4$ or $t = 1.5$, which corresponds to the time when the enstrophy reaches its maximum. After this time all modes of the system reach their maximum excitation and start decaying.

A comparison of the kinetic energy time dependence for the 128^3 PPM and 512^3 NS simulations, Fig. 10, led us to the conclusion that the PPM method requires roughly four times less resolution than NS to model the same system. If instead we compare the time histories of enstrophy, we conclude that PPM requires only a factor 2 less grid resolution.

We could not expect PPM and NS simulations to agree in all respects on any pair of grids, but we believe the evidence presented here clearly indicates that PPM delivers on the promise of Euler schemes to produce on a given grid better approximations to the infinite Reynolds number limit than can be obtained by using the Navier–Stokes equations at a finite Reynolds number.

The power spectra of velocity are represented in Fig. 11. The linear slope indicated by the straight line is the Kolmogorov $(-5/3)$ law. We can see that between wavenumbers $k_1 = 4$ and $k_2 = 32$ the highest resolution PPM spectrum shows the Kolmogorov inertial range law.

Here we define the inertial range to be the range of scales where the effects of any driving force, particular initial condition, geometrical boundaries, or small scale dissipation are negligible. We have no driving terms present here. The initial condition has a velocity

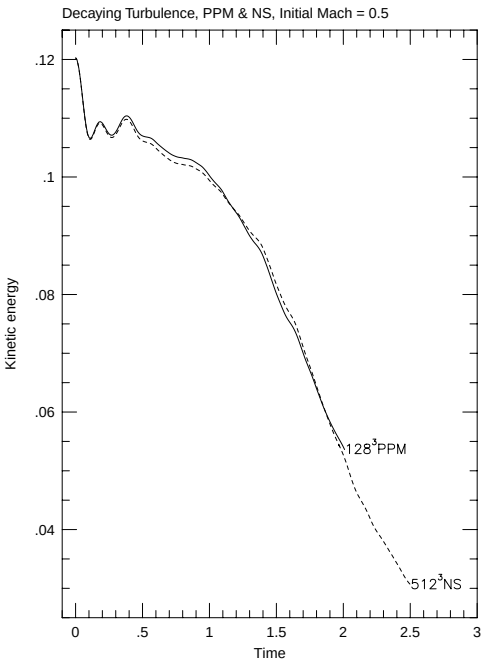

FIG. 10. A comparison of the kinetic energy time dependence for PPM and NS solutions. Decaying compressible turbulence. The initial Mach number is 0.5. The mesh size for Navier–Stokes solver is 512 zones per side of the cube and it is 128 zones for PPM solution.

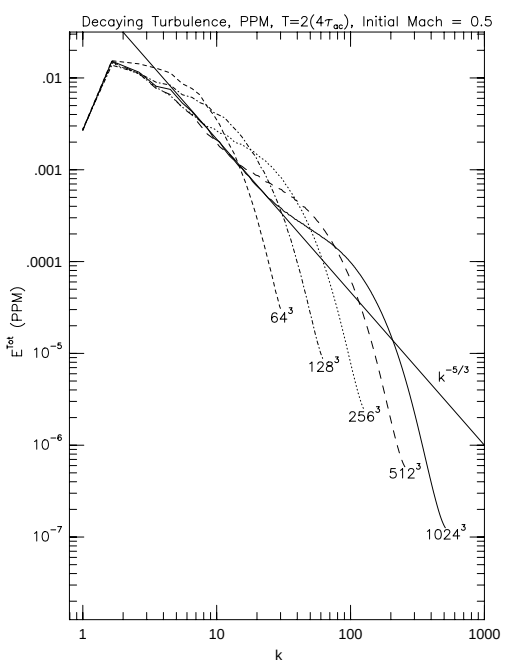

FIG. 11. A comparison of velocity power spectra in 5 PPM runs on progressively finer grids ranging from 64 to up to 1024 zones per side of the cube. The initial Mach number for all runs is 0.5. All spectra represent time $t = 2$ after 4 sound crossings of the energy containing scale. A line with a slope $k^{-5/3}$ represents Kolmogorov inertia range slope.

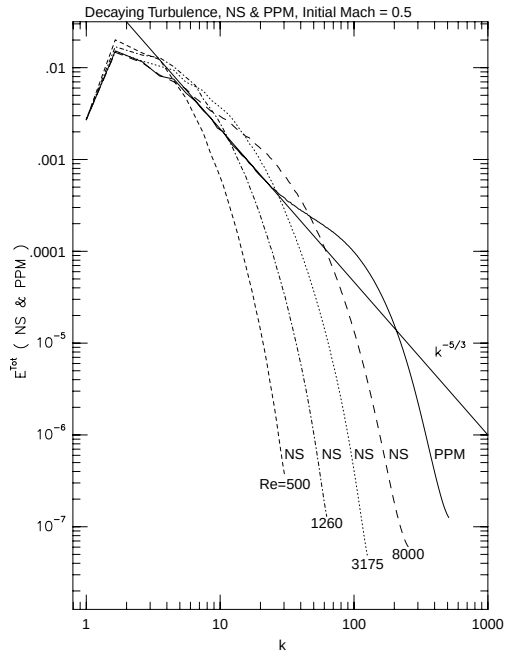

FIG. 12. A comparison of velocity power spectra in 4 NS runs on progressively finer grids ranging from 64 to up to 512 zones per side of the cube. The initial Mach number is 0.5. The PPM solution on the 1024^3 grid is presented for comparison. All spectra represent time $t = 2$ after 4 sound crossings of the energy containing scale. The line with a slope $k^{-5/3}$ represents the Kolmogorov inertial range slope. Reynolds numbers for the NS simulations reach 8000.

power spectrum $k^4 \exp(-k/k_0)^2$, with $k_0 = 2$, which places 99% of the energy in modes with k less than 4. Our boundaries are periodic and have little affect on the flow for modes with wavenumbers more than 8. The small scale dissipation in our modes is due to the numerical dissipation of the PPM and, for the 1024^3 grid, starts for modes with wavenumbers higher than 128 (Fig. 12).

On the smallest scales ranging from 2 to 12 times the width of computational cell, the numerical viscosity of the PPM code provides dissipation that directly dampens the fluid motion and converts kinetic energy into heat with total energy conserved to machine round-off precision.

Our tests of the convergence of the velocity power spectra as the computational mesh resolution is increased indicate that dissipative effects are negligible in the 1024^3 data filtered at $k = 32$ [4]. On large scales up to 32 cell widths PPM viscosity affects flow indirectly. An analysis of this effect can be found in [10].

Near the dissipation range the velocity power spectra display an approximate k^{-1} power law, which first was noted in [3]. The experimental data of Gagne obtained in the wind tunnel [11] as well as the work of other authors [13, 12] indicate similar behavior. Such accumulation of energy in small scales was not observed in our 2-D simulations [3], so one can see here the 3-D effect of the dynamics of vortex tubes near the dissipation scale.

We must point out that our NS run with mesh size 512^3 shows no significant inertial range. Therefore to obtain the separation of energy containing and dissipation ranges using NS one should use a mesh of at least 2048^3 and more likely of 4096^3 cells.

4. CONCLUSION

Our direct comparison of homogeneous decaying compressible turbulence modeled by using the PPM Euler method with Navier–Stokes calculations indicates that PPM can accurately simulate turbulent flow in a wide range of spatial scales.

Our convergence results for increasing Reynolds number indicate that 3-D Navier–Stokes flows with Reynolds numbers high enough to separate the energy containing and dissipation ranges in supersonic flow would require meshes of 2048^3 or larger, which are unattainable on present computers.

We wish to use the data from our simulation to test assumptions made in constructing turbulence closure models. Since these assumptions pertain to the Kolmogorov inertial range only, one needs to deal with data for which this range covers a reasonable interval in wavenumber and for which features pertaining to larger or smaller scales may be effectively and unambiguously filtered out. We concluded that PPM simulations on 1024^3 grid meet these requirements. Such simulations are the most efficient means we know to obtain unbiased "experimental" data from which appropriate statistical information can be extracted to guide theoretical modeling efforts for compressible turbulent flows in the limit of very high Reynolds numbers.

ACKNOWLEDGMENTS

The authors are pleased to acknowledge grants of computer time from the Los Alamos National Laboratory (LANL) and the National Center for Supercomputing Applications (NCSA) where the computations were performed. Very useful discussions with Tom Jones of the Astronomy Department, University of Minnesota, helped to keep us focused. The discussions and efforts of Laboratory for Computational Science and Engineering staff members Wenlong Dai and Steve Anderson were also helpful. This work was supported by the National Science Foundation, under Grand Challenge Grant ASC-9217394, by the Department of Energy by Grant DE-FG02-87ER25035, and through the Lawrence Livermore National Laboratory under the ASCI Project through Grant LLNL/B31627/DOE and the Los Alamos National Laboratory under Grant LANL/B33700016-3Y/DOE. This work was supported also by the National Center for Supercomputing Applications under Grant MCA97S006N. The LCSE, where the analysis of the data was performed, is also supported in part by a grant from the Minnesota Supercomputer Institute.

REFERENCES

1. D. H. Porter, A. Pouquet, and P. R. Woodward, Three-dimensional supersonic homogeneous turbulence: A numerical study, *Phys. Rev. Lett.* **68**, 3156 (1992).
2. D. H. Porter, A. Pouquet, and P. R. Woodward, A numerical study of supersonic homogeneous turbulence, *Theor. Comput. Fluid Dyn*. **4**, 13 (1992).
3. D. H. Porter, A. Pouquet, and P. R. Woodward, Kolmogorov-like spectra in decaying three-dimensional supersonic flows, *Phys. Fluids A* **6**, 2133 (1994).
4. P. R. Woodward, D. H. Porter, B. K. Edgar, S. E. Anderson, and G. Basset, Parallel computation of turbulent fluid flow, *Comput. Appl. Math*. **14**, 97 (1995).
5. P. R. Woodward and P. Colella, The numerical simulation of two-dimensional fluid flow with strong shocks, *J. Comput. Phys.* **54**, 115 (1984).
6. P. Colella and P. R. Woodward, The piecewise parabolic method (PPM) for gas-dynamical solutions, *J. Comput. Phys.* **54**, 174 (1984).
7. P. R. Woodward, Numerical methods for astrophysicists, in *Astrophysical Radiation Hydrodynamics* (Reidel, Dordrecht, 1986), p. 245.

8. P. R. Woodward, D. H. Porter, W. Yang, and Q. Mei, Simulation and visualisation of compressible convection in 2- and 3-D, in *Nonlinear Astrophysical Fluid Dynamics*, Annals of the New York Academy of Science (New York Acad. Sci., New York, 1990), Vol. 617, p. 234.
9. D. H. Porter and P. R. Woodward, High resolution simulations of compressible convection with the Piecewise-Parabolic Method, *Astrophys. J. Suppl.* **93**, 309 (1994).
10. D. H. Porter , P. R. Woodward, and A. Pouquet, Inertial rage structures in decaying compressible turbulent flows, *Phys. Fluids* **10**(1), 237 (1998).
11. Z.-S. She and E. Jackson, On the universal form of energy spectra in fully developed turbulence, *Phys. Fluids A* **5**, 1526 (1993).
12. V. Borue and S. Orszag, Forced three-dimensional homogeneous turbulence with hyperviscosity, *Europhys. Lett.* **29**, 687 (1995).
13. N. Cao, S. Chen, and Z.-S. She, Scalings and relative scalings in the Navier–Stokes turbulence, *Phys. Rev. Lett.* **76**, 3711 (1996).
14. M. Lesieur, *Turbulence in Fluids*, Fluid Mechanics and Its Applications (Kluwer Academic, Dordrecht, 1997), Vol. 40.
15. I. V. Sytine, D. H. Porter, and P. R. Woodward, A study of Reynolds stress and strain tensor components in 3-D homogeneous compressible turbulence, *Bull. APS* **43**(9), 1995 (1998).
16. I. V. Sytine, D. H. Porter, P. R. Woodward, and T. W. Jones, A study of subgrid stress tensor and energy dissipation rate in 3-D homogeneous compressible turbulence, Part II, *Bull. APS* **44**(1), (1999).
17. D. H. Porter, A. Pouquet, I. V. Sytine, and P. R. Woodward, Turbulence in compressible flows, *Phys. A* **263**, 263 (1999).
18. B. van Leer, Toward the ultimate conservative difference scheme, *J. Comput. Phys.* **54**, 115 (1976).
19. S. K.Godunov, Difference methods for the numerical calculation of the equations of fluid dynamics, *Mat. Sb.* **47**, 271 (1959).
20. W. G. Strang, On construction and comparison of differential schemes, *SIAM J. Numer. Anal.* **5**, 115 (1968).
21. G. L. Bryan, R. Cen, M. L. Norman, J. P. Ostriker, and J. M. Stone, X-ray clusters from a high-resolution PPM simulation of the cold dark matter universe, *Ap. J.* **428**, 403 (1994).
22. D. Dinge, Two-dimensional computational comparison of the dynamics interactions of critical and subcritical mass protoglobular cluster clouds with protogalactic background, *Ap. J.* **479**, 371 (1997).
23. S. T. Zalesak, Introduction to "Flux-corrected transport. I. SHASTA, a fluid transport algorithm that works," *J. Comput. Phys.* **135**, 170 (1997).
24. J. P. Boris and D. L. Book, Flux-corrected transport, *J. Comput. Phys.* **135**, 172 (1997).
25. J. Uthuppan, S. K. Aggarwal, and F. F. Grinstein, Particle dispersion in a transitional axisymmetric jet: A numerical simulation, *AIAA J.* **32**, 2004 (1994).
26. F. F. Grinstein, E. S. Oran, and J. P. Boris, Direct numerical simulation of axisymmetric jets, *AIAA J.* **25**, 92 (1987).
27. C. Fureby and S.-I. Moller, Large eddy simulation of reacting flows applied to bluff body stabilized flames, *AIAA J.* **33**, 2339 (1995).
28. C. Fureby, Large-eddy simulation of turbulent anisochoric flows, *AIAA J.* **33**, 1263 (1995).